ChemCatChem

ChemCatChem
Chemistry Europe
European Chemical Societies Publishing

RESEARCH ARTICLE OPEN ACCESS

DFT Study of Support Effects for O_2 Dissociation on Cu_5 Clusters: Opposite Trends in N-doped Graphene Compared to $CeO_2(111)$

Estefanía Fernández[1,2] | Joachim Paier[3] | Mercedes Boronat[1] | Joachim Sauer[3]

[1]Instituto De Tecnología Química (UPV-CSIC), Universitat Politècnica de València – Consejo Superior de Investigaciones Científicas, Valencia, Spain | [2]Departamento de Catálisis Aplicada, Instituto de Catálisis y Petroleoquímica, Consejo Superior de Investigaciones Científicas, C/ Marie Curie 2, Madrid, Spain | [3]Department of Chemistry, Humboldt-Universität zu Berlin, Berlin, Germany

Correspondence: Mercedes Boronat (boronat@itq.upv.es) | Joachim Sauer (js@chemie.hu-berlin.de)

Received: 22 October 2025 | **Revised:** 23 December 2025 | **Accepted:** 31 December 2025

Keywords: copper clusters | density functional calculations | heterogeneous catalysis | oxidation | supported catalysts

ABSTRACT

The metal-support interaction (MSI) effect of different supports, namely, N-doped graphene (N-graphene) and $CeO_2(111)$, on the properties of the planar 2D and 3D isomers of copper clusters of atomicity five was computationally studied at the PBE level (+U for Ce). For graphene-based systems, both pristine and defective sheets were considered. The stability, geometry and electronic properties of the supported Cu_5 clusters are discussed, and the dissociation of O_2 is studied on the most stable systems for both isomers. As expected, the interaction between Cu_5 and clean graphene or N-graphene is weak, and although adding nitrogen to graphene enhances the interaction, proper chemical adsorption is only achieved on the defects explored. In contrast, both Cu_5 isomers interact strongly with $CeO_2(111)$. The weaker MSI with N-graphene materials allows the deformation of the Cu_5 cluster upon O_2 adsorption, whereas $CeO_2(111)$ supported structures are more robust. O_2 dissociation on N-graphene-supported Cu_5 is consistent with our previous results on gas-phase clusters, i.e. the 2D isomer is more resistant to oxidation than the 3D one but the latter is more easily reducible, while on $CeO_2(111)$ this trend is reversed due to the strong MSI.

1 | Introduction

Copper is an available and cheap material that has generated great interest in recent years as potential substitute of noble metals in different catalytic applications [1, 2]. In the form of nanoparticles supported on metal oxides, copper is a promising catalyst for CO/CO_2 hydrogenation to methanol [3–9], CO oxidation [10–16] or the water gas shift reaction [17–19], among others [20–22], while graphene-based materials are preferentially selected as support for electrocatalysis and photocatalysis [23–25].

The catalytic activity and selectivity of copper nanoparticles depends largely on geometrical properties like particle size, shape, and degree of dispersion on the support, as well as on electronic features as the oxidation state, with irreversible oxidation to Cu^{2+} being the principal cause of deactivation in copper-based catalysts [1]. Decreasing the metal particle size to less than one nanometer produces small clusters composed by just a few atoms that exhibit new geometric, optical, and catalytic properties associated to their molecular-like electronic structure [2, 26–32]. Copper clusters in particular become more resistant to oxidation and also more easily reducible after oxidation than bigger nanoparticles [33–35]. Indeed, in previous studies from the group, we have computationally shown that copper clusters with 5 or less atoms favor planar morphologies, which are not able to activate O_2 as efficiently as 3D ones. As a result, the smallest

copper clusters are the most resistant to oxidation and the most prone to be reduced [33, 34]. These features are potentially useful to catalyze oxidation reactions, as we also reported with gas phase theoretical studies on CO oxidation [36], propene epoxidation [37] and partial methane oxidation to methanol [38].

However, going smaller has also the consequence of clusters being generally less stable: they tend to sinter into larger particles or decompose upon interaction with reactants, making size-specific clusters difficult to synthesize and apply, and even for a fixed atomicity they typically present a fluxionality that can similarly affect their activity [32, 39, 40]. To avoid these issues, different strategies to stabilize atomically precise clusters are tried, typically using ligands or solid supports, but also including confinement within metal-organic frameworks (MOFs) or zeolites [27, 28, 31, 41–43]. Inevitably, the interaction between the cluster and the stabilizers affects the metal particle properties to a certain degree, potentially changing the overall behavior of the material. As a result, this needed metal-support interaction (MSI) can also be regarded as an opportunity to tune the material toward optimal catalytic performance.

In this work, included as chapter five in Fernandez, E. PhD thesis [44] (https://doi.org/10.4995/Thesis/10251/135277), we explore and compare the metal-support interaction (MSI) in Cu_5 clusters stabilized on two very different materials: N-doped graphene with an expected minor influence on the properties of the supported clusters, and ceria (CeO_2) from which we do anticipate a larger MSI.

It is known that the band structure of graphene can be modified to suit many optical, electrochemical, or catalytic applications, either through the deformation of the sheet into nanoribbons or graphene quantum dots, or through dopants [25, 45–48]. In our case, as also pointed out by others [49], the N-doping of graphene was pursued to enhance the interaction between the sheet and the copper clusters, to avoid both the sintering of the latter and the modification of their properties. When nitrogen is introduced in graphene, a number of species can be formed, among which those known as graphitic N and pyridinic N are common [47, 48]. We decided to model sheets with both, since the latter involves a carbon vacancy defect that will likely act as a better anchor site for the clusters, much like it happens in undoped graphene [50, 51].

CeO_2 is a widely used support material for metal nanoparticles and clusters, as well as a catalyst itself due to its oxygen storage capacity [52–60]. The easy change in oxidation state of cerium ions between Ce^{4+} and Ce^{3+} not only facilitates the formation and healing of oxygen vacancies on its surface, but also the transfer of electrons from the supported metal species, generating new active sites on the partly cationic supported particles or at the metal-support interface [61]. Ceria is thus a reducible oxide far from inert, and there are many examples in the recent literature of optimized catalytic performance via tailored copper-ceria interactions. In particular, Cu/CeO_2 electrocatalysts with specifically designed Cu(II)-oxygen vacancy pair sites [62] and Cu-doped CeO_2 catalyst with frustrated Lewis pairs [63] have been reported to accelerate the slow water dissociation kinetics that limits the effective supply of protons during electrocatalytic CO_2 reduction, thus enhancing significantly their activity and selectivity to methane. Besides, Cu/CeO_2 catalysts have also shown improved selectivity to CO_2 in the preferential oxidation of CO in H_2-rich streams (CO-PROX) reaction [64] and to methanol in the CO_2 hydrogenation [65] thanks to a controlled MSI. In the field of pollution control, the abatement of volatile organic compounds (VOCs) using CeO_2-based catalysts requires a strong interaction between Cu(II) sites in CuO and Ce^{3+} ions in the CeO_2 support to achieve high activity, as illustrated for toluene oxidation by Zeng et al., [66]. And the strong MSI between highly dispersed Cu and CeO_2 nanostructures as hollow spheres or nanorods promoted again the generation of oxygen vacancies and ordered interfacial sites responsible for outstanding catalytic performance in low temperature WGS [67] or RWGS [68] reactions. It is clear, then, that the different types of MSI existing in each of these catalysts are crucial for their activity, but also that they are complex systems where support and metal are present in different forms and the effect of each of their features is not so easily disentangled. To take a first step toward this goal, we aim to understand how relevant is the influence of the support on some apparently simple structure-activity relationships.

Thus, in the present work, we model the 2D and 3D isomers of Cu_5 supported on representative graphene-based sheets and on the $CeO_2(111)$ surface, the usually predominant facet in ceria catalysts. Their structure, charge distribution and interaction with O_2 when supported on N-graphene and $CeO_2(111)$ are discussed and compared to previous gas phase results, showing that only the MSI on $CeO_2(111)$ is strong enough to reverse the relationship between cluster morphology and reactivity.

2 | Methods

All calculations in this work are based on Density Functional Theory (DFT), spin-polarized and using the functional of Perdew, Burke, and Ernzerhof (PBE) [69], and were carried out with the Vienna Ab-initio Simulation Package (VASP) [70, 71]. To partially remedy the self-interaction error (SIE) of the functional, which prevents electrons to correctly localize in Ce atoms when Ce^{3+} cations are formed, the *4f* orbitals of the Ce atoms are treated using the rotationally invariant approach to the DFT+U method, introduced by Dudarev et al., [72], with a Hubbard-type parameter of U_{eff} = 4.5 calculated by Fabris et al., [73]. using a linear response approach [74]. Note that no U value fits all properties accurately, but values in the 4.5-5.5 eV range provide a good qualitative electronic description of the ceria surface [52, 75]. The valence density was expanded in a plane wave basis set with a kinetic energy cutoff of 600 eV, and the effect of the core electrons in the valence electron density was considered by means of the projector augmented wave (PAW) formalism [76]. The electrons included in the valence space were $3p^6 3d^{10} 4s^1$ for Cu, $2s^2 2p^2$ for C, $2s^2 2p^3$ for N, $5s^2 5p^6 6s^2 5d^{14} f1$ for Ce and $2s^2 2p^4$ for O. The convergence criteria were 10^{-5} eV for the SCF energy and 0.02 eV/Å in the maximal forces per atom.

All graphene sheets were modelled by 8x8 supercells built from a graphene unit cell of a = b = 2.468, $\alpha = \beta = 90°$, and $\gamma = 120°$ used previously in the group [77], reoptimized at the PBE level. C and N atoms were removed and substituted, respectively, to create the corresponding defective and N-doped sheets, which were later reoptimized (allowing no changes to the cell). For the $CeO_2(111)$ surface, a 3x3 supercell slab model was employed to

support Cu_5, generated from a bulk model of a = b = c = 5.490 and $\alpha = \beta = \gamma = 90°$ (a larger 4x4 supercell was used to study alternative Ce^{3+} positions). The slabs contained 9 atomic layers (three O-Ce-O stacks), of which the top 6 were allowed to relax during optimizations. In all slabs periodic images were separated by a vacuum layer sufficiently large (20 Å for graphene sheets and about 14 Å for ceria). Isolated clusters and the O_2 molecule were optimized in a 15x15x15 $Å^3$ cubic box and integration in the reciprocal space was carried out at the Γ k-point of the Brillouin zone. The Γ k-point was also enough for graphene and 4x4 ceria slabs, whereas a 2x2x1 k-points mesh generated with the Γ–centered Monkhorst-Pack algorithm [78] was used for the 3x3 slabs. The Gaussian smearing method was employed to determine electron occupancies with a smearing parameter of σ = 0.02 eV, which was increased to 0.05 eV to evaluate the band structure of graphene sheets, together with an increased 12x12x1 k-points mesh.

Vibrational frequencies were calculated numerically through central differences of analytically calculated forces, as implemented in VASP, in partial hessian calculations where the whole slab was fixed. Atomic charges were obtained through the Bader charge analysis [79–81], whereas magnetization, spin densities, and density of states (DOS) data were obtained through the projection of the wavefunctions onto spherical harmonics centered at the position of the ions. Dispersion interactions were taken into account by adding atom pair 1/R6 terms as parameterized by Grimme (DFT+D2) [82] throughout the optimization for graphene systems, whereas only single-point calculations were done at the PBE+U structures on ceria. For the C and R0 parameters, values of 20.00 and 1.860 were chosen for Ce, which were previously calculated and tested [83], and default parameters were adopted for the other atoms (10.80 and 1.562 for Cu, 0.70 and 1.342 for O, 1.75 and 1.452 for C and 1.23 and 1.397 for N). Transition states were located using the Improved DIMER [84, 85] or CI-NEB [86] algorithms. In addition, the Jmol [87] and p4vasp [88] programs were used to build and visualize the systems and their frequencies throughout the work, whereas VESTA [89] and QtGrace [90] were employed to obtain the images of structures and DOS, respectively.

3 | Results and Discussion

3.1 | Supported Cu_5 Clusters

3.1.1 | Cu_5 on Graphene-Based Supports

The planar 2D and 3D isomers of Cu_5 known from previous works [33, 34] (Figure 1d) were placed on four different graphene-based sheets. Both pristine and one-carbon-defective sheets were considered, labelled G and G_V for graphene, and NG and NG_V for N-graphene (Figures 1a,b, and S1). To compare with the previous experimental results [34], a 10% amount of nitrogen was targeted for N-doped models. Thus, NG is a clean sheet with graphitic N atoms only (N_{Gr}), while NG_V additionally contains three pyridinic N atoms neighboring the C vacancy (N_{Py}). Note that G and Gv were studied in this section only, to assess the enhanced cluster stability expected from the employment of N-graphene in the experimental samples.

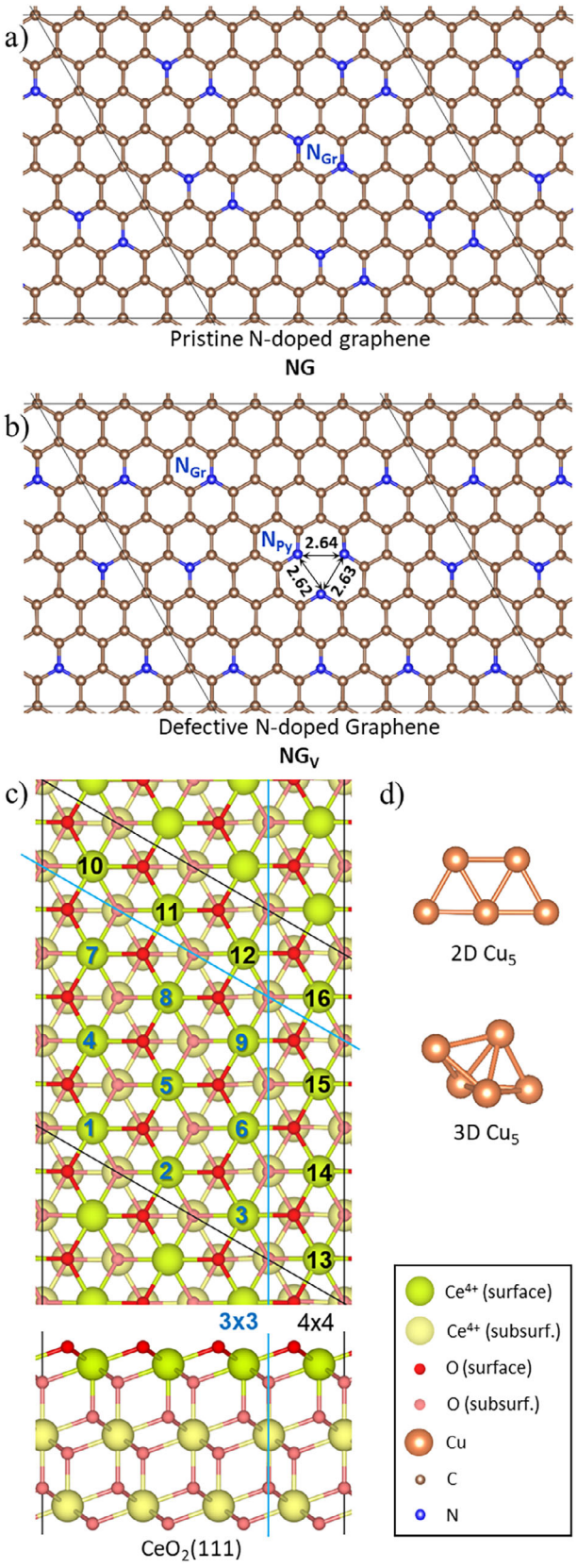

FIGURE 1 | a-b) N-graphene and c) CeO_2(111) surface models employed (see also Figure S1) and d) Cu_5 isomers considered. Periodic cells are indicated by straight lines. Interatomic distances at the C vacancy are indicated in Å. Atom color labeling shown in legend. Surface Ce atoms are numbered for reference.

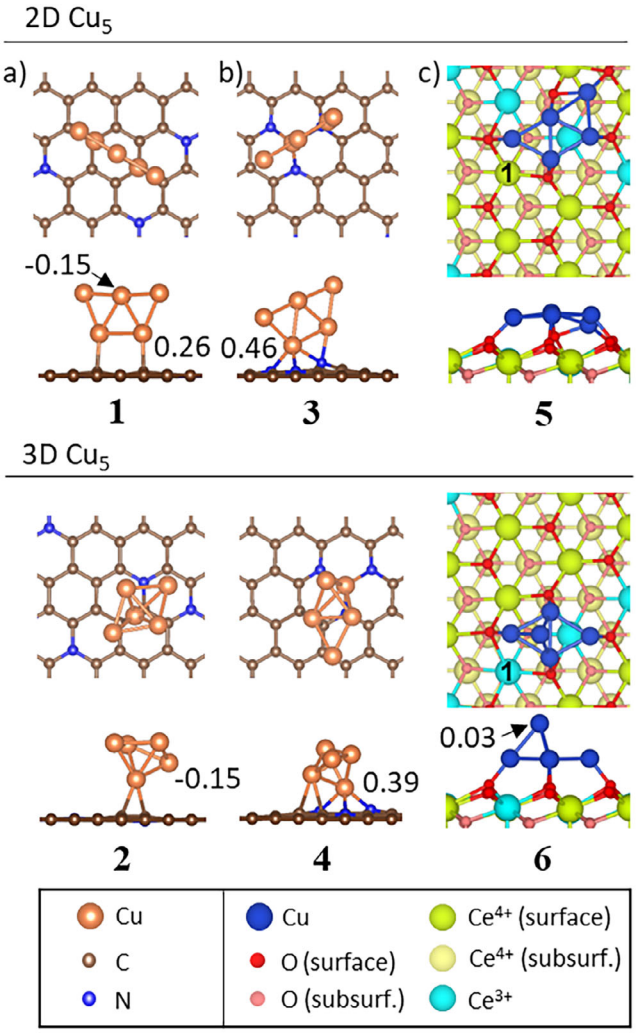

FIGURE 2 | Most stable structures of 2D Cu_5 (top) and 3D Cu_5 (bottom) clusters supported on a) NG, b) NG_V, and c) $CeO_2(111)$. Top and side views are shown. Atom color labeling shown in legend. Bader charges on some copper atoms are specified.

The differences between these graphene sheets are reflected in their PDOS (Figure S2) and their Bader charges (Figure S3 and Table S1). N_{Gr} are saturated, and since nitrogen has one more electron than carbon, they start to fill the π^* band, introducing n-type doping in the system. C vacancies imply one less electron in the π band but, more importantly, the atoms neighboring it (such as N_{Py}) become unsaturated. As a result, they have both the geometrical and electronic space to undergo sp^3 hybridization and form bonds. Consistent with this description of the graphene sheets, copper clusters avoid the graphitic N atoms of N-graphene upon adsorption (Figures 2, S4 and S5) and adsorb more strongly on the vacancies of defective sheets (Figures 2 and S6). Thus, clusters adsorbed in G_V, the most unstable system due to its unsaturated C atoms, present the largest adsorption energies (-107.7 and -113.3 kcal mol^{-1}, Table S4) followed by NG_V (-73.8 and -82.2, Tables 1 and S5). The adsorption energy for structures on G or NG are at least 50 kcal mol^{-1} higher, ranging from -27.2 to -38.5 kcal mol^{-1} and being 6-11 kcal mol^{-1} better in the N-doped sheet (Tables 1, S2 and S3).

The adsorption is also reflected in the charge transferred between the cluster and the support. In many structures the Bader analysis reveals that the copper atoms at the interface are positively charged, whereas atoms in the external surface of the cluster exhibit up to -0.3e negative charge (Figures 2 and S4–S6). In most cases the net effect is for the cluster to give charge to the support, between 0.1 and 0.4e for clean sheets and significantly larger, between 0.3 and 1.0e, for defective ones (Tables 1 and S2, S3). However, in a few isomers and on clean sheets only, small negative charges are found on the clusters, i.e. the support loses charge in favor of the cluster. The most remarkable cases would be those of 3D Cu_5 on G and NG (structures **S11** and **2**), which present -0.2 and -0.1e total charge, respectively, and that are, in addition, the most stable structures found for that isomer in those supports.

Deformations on the clusters upon optimization are larger on the defects due to the higher interaction strength, which overcomes the cluster resistance to deformation. Structure **4** on NG_V, for instance, exhibits a 3D-like isomer that resembles a tetrahedral Cu_4 with an additional atom on one edge, and it was obtained from an initially planar cluster that deforms during the optimization (Figure 2). In most other cases, Cu_5 isomers largely retain their characteristic 2D or 3D geometries (Figures S4–S6). Planar Cu_5 clusters preferentially adsorb vertically by the two atoms edge opposite to the three atoms edge, and 3D Cu_5 clusters interact through one or more of the central atoms of its bipyramidal shape, regardless of the type of graphene sheet. This correlates with the shape of the HOMO and LUMO for 2D Cu_5 and 3D Cu_5, which are highly localized in those areas (Figure S7), and also with the charge transfer from the cluster to the support found. The reversed charge transfer exceptionally found for structures **S11** and **2** of 3D Cu_5 is also explained by the lower energy of the LUMO of the 3D isomer, which facilitates the interaction, and its localized shape on top of one central atom, which is consistent with the fact that in those structures the cluster binds to graphene through one copper atom only.

Among the two isomers, 2D Cu_5 presents the highest adsorption energy only on the NG sheet, but given that the gas phase 3D isomer is 6 kcal mol^{-1} less stable than the planar one, 2D Cu_5 is still thermodynamically favored over all but the pyridinic NG_V sheet (Table 1). Even there it remains close, 2.4 kcal mol^{-1} below. The largest difference lies in the NG sheet, where the most stable planar cluster is 8.2 kcal mol^{-1} more stable than the most stable 3D structure. Therefore, while not clearly dominating, planar clusters are favored on NG, whereas pyridinic defects favor 3D clusters and may moreover deform the planar isomer into the 3D one.

3.1.2 | Cu_5 on the $CeO_2(111)$ Surface

In this case, the strength of the metal-support interaction induces structures where the copper clusters match the high symmetry of the $CeO_2(111)$ surface, and we found very few isomers close in energy to the lowest energy structures (Figures 2 and S8 and Tables 1 and S6).

The geometry of the cluster in structure **5** (Figure 2c) is very similar to that of the most stable planar structure for Cu_5 found in gas phase, but it lies now flat with all its atoms in contact with the surface, and with one of the less-coordinated copper atoms

TABLE 1 | Adsorption energies with respect to each isomer of Cu_5 clusters on NG, NGV, and CeO_2(111) (ΔE_{ads}), relative energies (ΔE_{rel}), Bader charges on the cluster (qCu_5), and Ce^{3+} positions. PBE+D2 energies in kcal mol^{-1}.

Support	Isomer	Struc. (Figure 2)	ΔE_{rel}	ΔE_{ads}	qCu_5 (e^-)	Ce^{3+} pos.
Gas phase[a]	2D Cu_5		0.0			
	3D Cu_5		6.3			
NG	2D Cu_5	1	0.0	−38.5	0.11	
	3D Cu_5	2	8.2	−36.3	−0.11	
NG_V	2D Cu_5	3	2.4	−73.8	0.47	
	3D Cu_5	4	0.0	−82.2	0.45	
CeO_2(111)	2D Cu_5	5	0.0	−142.6	1.53	4, 5, 6
	3D Cu_5	6	1.4	−147.2	1.38	1, 5, 9

[a]From our previous work [33].

slightly bent inwards, from where an oxygen atom also moves to provide a better Cu-O interaction. In structure **6** the geometry is that of the open 3D Cu_5 already seen on graphene, with one of the Cu-Cu bonds broken. These constitute the largest deformations found on ceria. Indeed, the deformation of the copper isomers on metal oxides is influenced by the matching between the surface oxygen atoms and the copper atoms. For instance, the more inert γ-Al_2O_3(110) breaks 2D Cu_5 into two Cu_3-Cu_3 that share a copper atom [91], and both γ-Al_2O_3(110) and TiO_2(110) preserve the gas phase 3D Cu_5 morphology due to their more corrugated surface [91, 92].

The strong metal-support interaction on ceria is reflected in high adsorption energies, about 65 kcal mol^{-1} higher than those on NG_V (Table 1). The 5 kcal mol^{-1} larger adsorption energy of 3D Cu_5 with respect to planar Cu_5 is remarkable considering it has one less Cu-O bond, but the two structures are still practically equally stable thermodynamically (within 2 kcal mol^{-1}, Table 1).

In addition, the reduction of some Ce^{4+} to Ce^{3+} is expected from the oxidation of the cluster. We find that the MSI is strong enough to break the closed shell electronic structure after the loss of the first unpaired electron, so that another two electrons can be transferred to the surface. This way, we find that on the most stable structures three Ce^{3+} ions are produced, with a corresponding Bader charge of around 1.5e (Table 1). Regarding charge distribution within the clusters, again atoms in contact with the surface are in general more positively charged, whereas the external ones tend to preserve their neutral metallic character or even become slightly negatively charged (<0.1e). This is especially evident in what one could call the bi-layered structure that constitutes the most stable structure of 3D Cu_5, where the atoms of the first layer are averagely charged by 0.34e, while the one on top presents a Bader charge of 0.03e.

The specific position of the reduced cerium cations can be detected by inspection of the spin density, looking for the singly occupied *4f* states (Figure S9). It was found that the specific position of a Ce^{3+} can change the energy of the system by as much as 0.5 eV, and that bigger cells may be needed to properly explore all possibilities. Nevertheless, our 3x3 and 4x4 tests show that the planar and 3D isomers of Cu_5 are close in energy, and a more or less even distribution of them should be expected (Figure S10).

These Ce^{3+} can also be found in PDOS as defects in the former surface gap of ceria, constituting now the highest energy occupied bands (Figure S11). Copper *3d* states can also be seen, and bands corresponding to the 3D Cu_5 cluster are significantly deeper below the Fermi level than those of the planar isomer, indicating a higher resistance to further oxidation. By the same token, the empty *3d* states of 3D Cu_5 are much closer to the Fermi level, which should translate in a higher reducibility for this isomer.

3.1.3 | O_2 adsorption on Supported Cu_5 Clusters

We modelled the adsorption of O_2 in the most stable structures for 2D and 3D Cu_5 on the two N-doped sheets and CeO_2(111), i.e. in those shown in Figure 2.

In agreement with previous studies [58, 93, 94], modelling molecular oxygen on the bare support surfaces shows very small adsorption energies, ranging from -0.3 to -8.8 kcal mol^{-1} (Figure S12 and Table S7). Consistent with this weak interaction, the O_2 molecule preferentially adsorbs on the copper cluster in all supported Cu_5 structures (Figures 3 and S13–S16 and Tables 2 and S8–S11), and those built with O_2 at the metal-support interface either evolve to other structures or are unstable (structures **S96** and **S120**).

Adsorption modes studied in gas phase copper clusters in our previous work [33] are found again here in all supports (Figures 3, 4 and S13–S16). Thus, we have *mono* modes when only one bond is formed between one of the O atoms of O_2 and a Cu atom (structure **S75**, for instance); *top*, when the two O atoms of O_2 are directly attached to the same low coordinated Cu atom (as in structure **S74**); *bridge*, when each of the two O atoms in the molecule is directly attached to one Cu atom in the cluster (structure **7**) and *h-111* when the O_2 occupies the hollow position on a {111} facet (structure **9**). An additional mode was obtained, which we labelled *mono-bridge* because the O atom bonded to copper in what would be a *mono* structure bridges two Cu atoms instead (structure **S73**).

The relationships between charge transferred to the oxygen molecule and its O-O distance and frequency vibration follow the expected trends reported previously [33] (Figure 4). Thus,

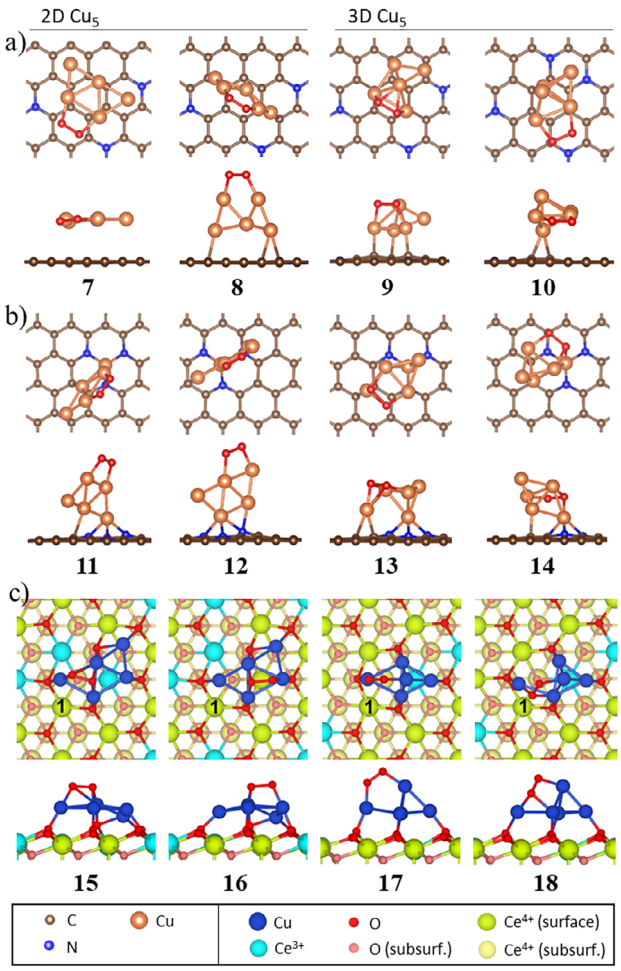

FIGURE 3 | The two most stable structures found for the O_2 molecule adsorbed on 2D Cu_5 (left) and 3D Cu_5 (right) supported on a) NG b) NG_V, and c) CeO_2(111). Top and side views are shown. Atom color labeling shown in legend.

h-111 modes present the highest activation of the O_2 molecule, with bond distances in the 1.45-1.58 Å range and corresponding vibrational frequencies from 589 to 785 cm^{-1} and -(0.81, 1.12)e Bader charges, followed by *bridge* modes (1.35-1.46 Å, 733-985 cm^{-1} and -(0.54, 0.95e)), and then by *mono* modes (1.29-1.33 Å, 1115-1214 cm^{-1} and -(0.43, 0.57)e). The new *mono-bridge* structures lie precisely between the *bridge* and *mono* modes, with 1.34-1.39 Å bond distances, 920-1045 cm^{-1} vibrational frequencies and -(0.65, 0.86)e Bader charges, much like the few *top* modes found (1.31-1.43 Å, 895-1182 cm^{-1} and -(0.41, 0.87)e).

In other words, the activation of the O_2 molecule is determined by its adsorption mode: it stabilizes as a *superoxo* species (O_2^-, Bader charges in the -(0.5-0.9)e range) in all but the more activated *h-111* modes, where it can become a *peroxo* (O_2^{2-}, Bader charges around -1e). Then, the activation of the *superoxo* species follows the adsorption trend *mono* < *mono-bridge* ≤ *top* < *bridge* < *h-111*.

On NG and NG_V, we find that the planar cluster preferentially adsorbs O_2 as *bridge* modes at its edges, whereas the 3D cluster additionally stabilizes *h-111* adsorption modes (Figure 3a,b). This result is qualitatively equivalent to our previous results on gas phase clusters. In fact, note that the 2D geometry evolves to interact with the O_2 molecule, as in gas phase, through the two Cu atoms edge, which previously was facing the surface.

On CeO_2(111), however, since the planar cluster is now flat, the *bridge* modes along the edges are now unstable (as in structure **S112**, Figure S15). Instead, the planar isomer favors now the adsorption of O_2 on its {111} facets, a feature impossible in gas phase planar Cu_5, and with a large adsorption energy (structures **15-16** and **S106-S107**). This critical change in the preferred adsorption mode and site is explained by looking at the highest occupied defect of mainly Cu *3d* character observed in the PDOS of 2D Cu_5/CeO_2(111), which spreads upwards and along one of the internal Cu-Cu bonds (Figure S17). In addition, this type of adsorption facilitates the formation of O-Cu-O quasilinear bonds that are typically favored by Cu^+, which probably contributes to the stabilization of the structure (see also Figure S15 and its discussion for details). The charge transferred to O_2 in these most stable planar Cu_5 structures comes from the cluster, and the same amount of pre-existing Ce^{3+} are found (Tables 2 and S10). For 3D Cu_5, however, one Ce^{3+} is always reoxidized (Tables 1 and S11). For N-graphene supports, in general, the charge gained by the molecule does not match the charge lost by the cluster either, i.e. the support participates: both the cluster and the support lose charge upon the adsorption of O_2 (Tables 2, S8 and S9). The degree of activation of the oxygen molecule still responds to the adsorption mode it is in regardless of the type of support, but to achieve it the cluster gets considerably more oxidized on the NG_V sheet for the same adsorption modes (Figure S18).

Another difference between the supports is that on N-graphene-based surfaces the interaction is weaker but stabilizing enough to facilitate deformations of the cluster upon O_2 adsorption. Some planar structures evolved upon optimization into 3D isomers and vice versa (see Figures S13 and S14 for details), which indicates that such conversions are likely affordable for the system. Thermodynamically, on the one hand, the adsorption of O_2 is stronger in the 3D clusters on NG_V, and ultimately produces lower relative energy values, favoring this isomer over the planar cluster (Table 2). On the other hand, the most stable planar structure over NG was 8.2 kcal mol^{-1} more stable than the 3D most stable structure (Table 1) and after O_2 adsorption the structures differ by 5 kcal mol^{-1} only (Table 2).

All in all, we can point out that: i) the planar isomer is more favored (thermodynamically) than the 3D one on all supports but the NG_V sheet, and the difference is largest on NG, ii) upon O_2 adsorption, 3D structures become more favored, especially on NG_V, and iii) interconversion of isomers seems to be affordable in both directions for N-graphene supports, but not on ceria due to the strong MSI.

As a result of this, and given that the isolated 3D isomer is 6 kcal mol^{-1} higher in energy than the planar one, neither isomer is expected to obtain a very high predominance over the other on N-graphene sheets. The data suggests that NG is the surface of choice in order to favor the planar isomer as much as possible but, given the low adsorption energies of all copper clusters on NG, very low loadings would still be needed to favor dispersion and avoid sintering, as it was precisely done for the samples in the experiments of our collaborators [34]. Then, since the planar isomer does not adsorb molecular oxygen in the more

TABLE 2 | Adsorption energies of O_2 on NG/NG_V- and ceria-supported clusters (ΔE_{ads}), relative energies (ΔE_{rel}), O-O distances (r_{OO}), O-O vibrational frequencies (ν_{OO}), Bader charges on the molecule (qO_2), cluster charge increase (ΔqCu_5) and Ce^{3+} atomic positions (numbering in Figure 1) for the structures in Figure 3. PBE+D2 energies in kcal mol^{-1}.

Support	Isomer	Struc. (Figure 3)	Ads. mode	ΔE_{rel}	ΔE_{ads}	r_{OO}[a] (Å)	ν_{OO}[a] (cm^{-1})	qO_2 (e^-)	ΔqCu_5 (e^-)	Ce^{3+} pos.
Gas phase[b]	2D Cu_5		*bridge*	0.0	−49.4	1.393	939	−0.75	0.75	
	3D Cu_5		*h–111*	16.2	−39.5	1.504	674	−1.03	1.03	
NG	2D Cu_5	7	*bridge*	5.2	−39.9	1.437	768	−0.95	0.53	
		8	*bridge*	5.7	−39.4	1.389	942	−0.67	0.46	
	3D Cu_5	9	*h–111*	0.0	−53.3	1.559	654	−0.94	0.92	
		10	*bridge*	8.6	−44.7	1.459	733	−0.73	0.43	
NG_V	2D Cu_5	11	*bridge*	12.7	−37.0	1.377	935	−0.70	0.45	
		12	*bridge*	24.4	−25.3	1.361	971	−0.63	0.45	
	3D Cu_5	13	*h–111*	0.0	−47.2	1.578	589	−1.03	1.05	
		14	*h–111*	6.6	−40.7	1.527	618	−0.94	0.72	
CeO_2(111)	2D Cu_5	15	*h–111*	0.0	−56.8	1.540	625	−1.09	1.04	3, 4, 6
		16	*h–111*	4.1	−52.7	1.544	629	−1.08	1.06	3, 4, 7
	3D Cu_5	17	*bridge*	13.4	−44.8	1.369	985	−0.73	0.39	5, 9
		18	*h–111*	13.8	−44.4	1.451	785	−0.87	0.36	5, 9

[a]For the gas phase O_2 molecule: $r_{OO} = 1.233$ Å, $\nu_{OO} = 1566$ cm^{-1}.
[b]From our previous work [33].

activated *h-111* mode, the Cu_5/N-graphene system should be more resistant to oxidation. In contrast, planar clusters adsorb stretched out over ceria, adsorbing O_2 in highly activated *h-111* modes, whereas 3D clusters are deformed upon adsorption and favor less activated *bridge* adsorption modes, precisely reversing the results obtained for gas phase and N-graphene-supported clusters.

3.1.4 | O_2 dissociation on Supported Cu_5 Clusters

The most stable structures of 2D and 3D Cu_5 with O_2 adsorbed in *bridge* and *h-111* modes were tested for O_2 dissociation (Figure 5 and Table 3). Structures **7** and **8** were selected for the planar isomer on NG. Both present O_2 adsorbed in a bridge mode and are very close in energy, but the comparison is interesting because while the former seems to activate O_2 a bit more, the latter has less contact with the surface. For the 3D isomer on NG, structures **9** (*h-111*) and **10** (*bridge*) were selected and, in the case of NG_V, we studied structures **11** and **13** for the planar and 3D isomers, respectively (also structure **S88** for its singularity, see Figure S19). Finally, on ceria, for planar Cu_5 structure **15** was considered, and for 3D Cu_5, the close in energy *bridge* and *h-111* modes of structures **17** and **18** were both explored.

From structure **7**, a TS with the two oxygen atoms separated and stabilized by the support was readily found, leading to a product where such stabilization produces actual bonds between the oxygen atoms and the carbon atoms of the surface (structure **19**), which clearly become sp^3 hybridized and move upwards with respect to the plane of the sheet. The activation energy from structure **7** is moderately high (25.9 kcal mol^{-1}), consistent with the lower activation of the *bridge* mode (Table 3). The fact that the cluster lies down on its face in principle maximizing the copper-surface interactions and yet standing a bit apart (resembling to float), raised the question of whether the addition of dispersion forces in the optimization was key to stabilize the structure. However, the reoptimization of the structures without dispersion forces was achievable and lead to a very similar activation energy (23.7 kcal mol^{-1}), even though the separation of the cluster from the surface is immediately visible by how it becomes tilted, with the O_2 still facing the surface but at a 0.25 Å larger separation (Figure S20).

From structure **8**, we did not succeed in converging a structure with the two oxygen atoms separated as before, but a TS where they move toward more stable bridge positions, much like for gas phase clusters, was achieved ($\mathbf{TS_{8\rightarrow 20}}$). The activation energy is similar but slightly higher (28.3 kcal mol^{-1}), consistent with the absence of stabilization from the interaction of the O with the support that the **7**→**9** path had, and fully in agreement with the result obtained for the gas phase 2D Cu_5, which showed precisely the same geometries for the initial state and TS structures (Table 3).

Regarding the 3D isomer on NG, although in structure **9** the O_2 molecule is adsorbed in the {111} facet of the cluster, it is easy to see that it is oriented so that it creates four O-Cu interactions. As a result, the activation of the molecule is a bit higher than in other *h-111* modes, becoming closer to what would be obtained in a proper *h-100* mode [33] (Table 2 and Figures 3 and 4). Consistent with this, the activation energy from this structure is much lower than from the *bridge* mode of 3D structure **10** (1.9 vs 18.7 kcal mol^{-1}, Table 3).

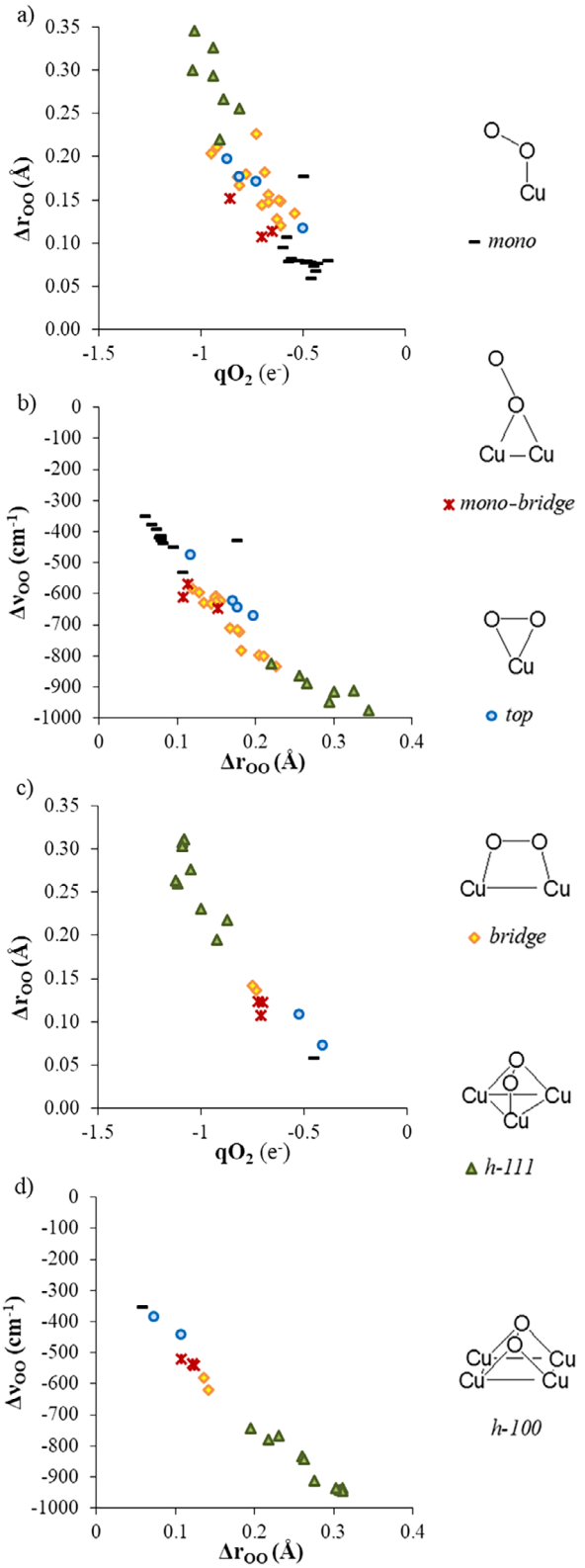

FIGURE 4 | Relationship between the bond length variation, Δr_{OO}, and the charge transferred, qO_2, (a,c) and between the shift in the vibrational frequency, $\Delta\nu_{OO}$, and the bond length variation, Δr_{OO}, (b,d) per adsorption mode on NG/NG_V (a,b) and CeO_2(111) (c,d): *mono* (black lines) *top* (blue circles) *bridge* (yellow diamonds) *h-111* (green triangles) and *mono-bridge* (red crosses). The *h-100* mode has been added to the legend scheme for clarity, although no such modes are reported here. Data from Tables S8 and S9 (top) and S10 and S11 (bottom).

On NG_V, in $\mathbf{TS_{11\to23}}$ the planar cluster slightly deforms to produce more Cu-C interactions and the oxygen atoms are monocoordinated to one Cu atom each, like in $\mathbf{TS_{7\to19}}$. The activation energy is more similar to that of $\mathbf{TS_{8\to20}}$, which is higher, definitely showing that the interaction of the O atoms with the graphene surface in $\mathbf{TS_{7\to19}}$ is what lowers the barrier, not the O atoms being placed at the shared Cu-Cu edge ($\mathbf{TS_{8\to20}}$).

From structure **13**, as expected again from its similarity to an *h-100* mode [33], the barrier is much lower (2 kcal mol^{-1}, Table 3). Indeed, both the initial and TS structures present an almost detached Cu atom that bonds to the rest of the cluster mainly through the two O atoms, exhibiting a total of four O-Cu interactions. Thus, the O_2 is initially more activated but also the TS is quite stable, both facts contributing to a lower activation energy.

Similarly, on ceria, the high activation of the O_2 molecule in the *h-111* modes on the planar cluster causes a low activation energy for O_2 dissociation (structure **15**, 9.6 kcal mol^{-1}, Figure 5e and Table 2), whereas that from the less activated *bridge* mode is higher (structure **17**, 25.1 kcal mol^{-1}). TSs from structures **17** and **18** were difficult to find, presumably because the oxygen atoms do not find enough Cu-O interactions to be stable, but also because O_2 and the copper atom on top allow the displacement of the copper atoms below. Eventually, the TS from structure **17** evolved toward an *h-111* mode ($\mathbf{TS_{17\to26}}$), much like for the *bridge* mode of 3D Cu_5 in gas phase [33]. The $\mathbf{TS_{18\to26}}$ obtained from structure **18** is similar, with one of the O atoms monocoordinated and the other on a Cu-Cu bridge. However, this second O atom does not achieve the same stabilization as in $\mathbf{TS_{17\to26}}$, where a third Cu-O interaction was observed. This is reflected in barriers of 25.1 and 20.6 kcal mol^{-1}, respectively (Table 2), and it explains why the activation energy from structure **18** is still high for an O_2 molecule adsorbed in an *h-111* mode, even in spite of the high activation of the O-O bond. With that exception, the values are in the range found for the same adsorption modes on N-graphene-supported clusters and further confirm that the activation of the O_2 molecule largely depends on its adsorption mode, now regardless of the copper cluster isomer it is achieved through. However, it also shows that the reactivity of the cluster for a given morphology can be severely changed via the MSI, for in Cu_5/CeO_2(111) systems the planar cluster is more active for the dissociation of O_2 than the 3D isomer; exactly the opposite result to what is found for gas phase and N-graphene-supported clusters.

Regarding the final state structures, in gas phase, oxygen atoms generally preferred to adsorb bi-coordinately to the copper atoms occupying *bridge* sites on 2D structures, and both *bridge* and *h-111* tri-coordinated facet sites on 3D Cu_5 [33]. On N-graphene, the oxygen atoms generally prefer *bridge* sites for both isomers, because the 3D cluster deforms a bit into structures that favor this type of adsorption (structures **21, 22** and **24**). In planar structures, tri-coordinated O atoms almost within the cluster are also observed (structure **20** and **23**), a geometry already found in previous works on gas phase [36, 37] or within zeolites [38, 41, 42]. In spite of these small differences, reaction energies are clearly negative, showing that the process is exothermic, in agreement with gas phase results. Furthermore, we observe again that, as in gas phase, the recombination of O_2 from two O atoms, that is, the reduction of the cluster, is easier for the 3D cluster (Table 3 and

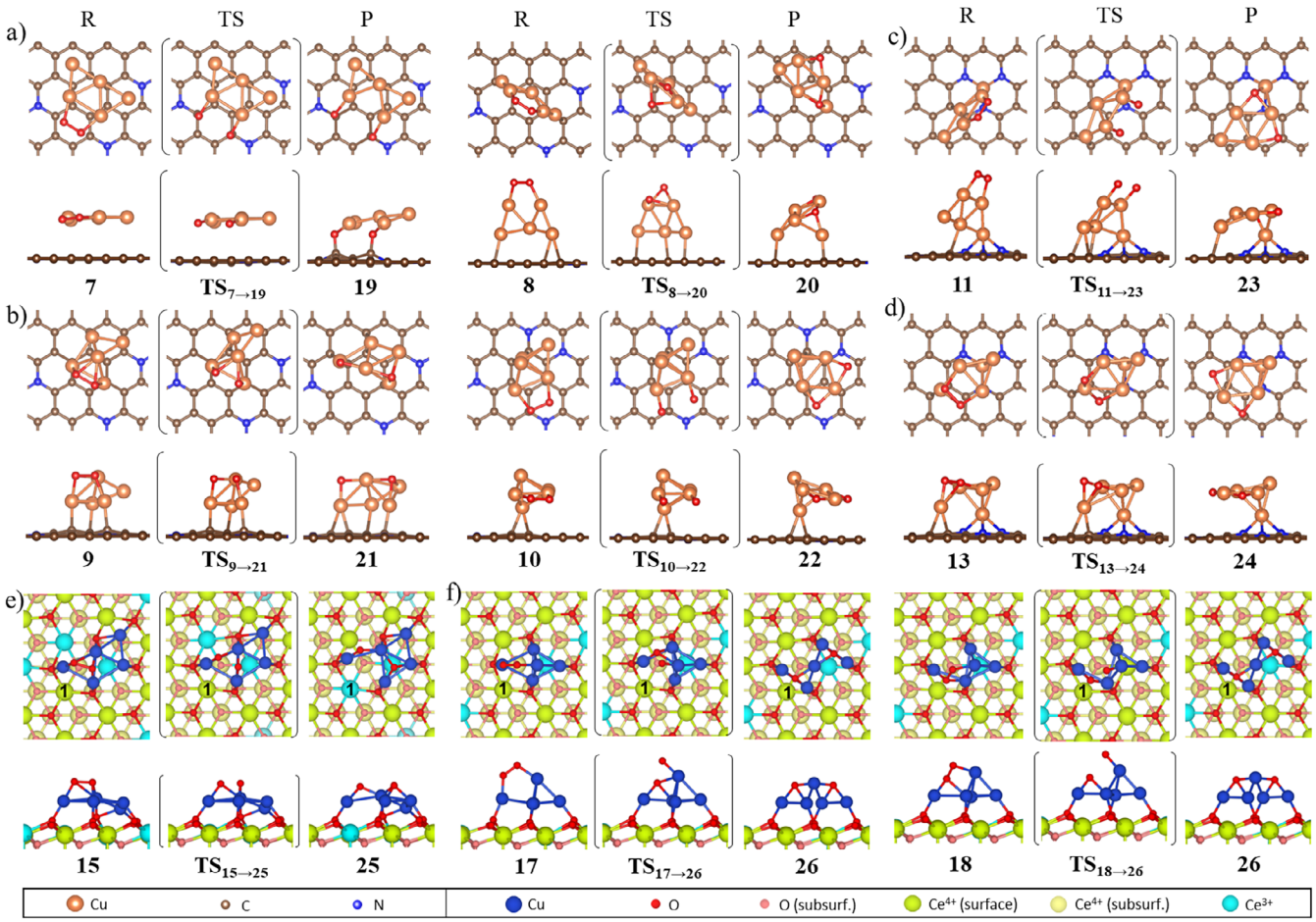

FIGURE 5 | O_2 dissociation by the most stable structures on the 2D (a,c,e) and 3D (b,d,f) isomers of Cu_5 on NG, NG_V and CeO_2(111), respectively. Top and side views are shown. Atom color labeling shown in legend.

TABLE 3 | O_2 adsorption energies on supported Cu_5 clusters (ΔE_{ads}), O_2 dissociation activation energies (ΔE_{act}), O-O distances in TS (r_{OO}(TS), in Å), reaction energies (ΔE_{reac}) and recombination energies (ΔE_{reco}). PBE+D2 energies in kcal mol^{-1}.

Support	Isomer	Path	ΔE_{ads}	ΔE_{act}	r_{OO}(TS)	ΔE_{reac}	ΔE_{reco}
Gas phase[a]	2D Cu_5		−49.4	30.8	1.969	−42.3	73.1
	3D Cu_5		−39.5	6.2	1.874	−55.6	61.8
NG	2D Cu_5	7→19	−39.9	25.9	2.643	−47.2	73.1
		8→20	−39.4	28.3	1.913	−59.2	87.5
	3D Cu_5	9→21	−53.3	1.9	1.827	−58.0	59.9
		10→22	−44.7	18.7	2.471	−58.1	76.8
NG_V	2D Cu_5	11→23	−37.0	28.3	2.394	−63.4	91.4
	3D Cu_5	13→24	−47.2	2.0	1.817	−45.7	47.7
CeO_2(111)	2D Cu_5	15→25	−56.8	9.6	1.777	−20.8	30.4
	3D Cu_5	17→26	−44.8	25.1	2.000	−77.5	102.6
		18→26	−44.4	20.6	2.336	−77.8	98.5

[a]From our previous work [33].

Figure 6). Given the deformations shown throughout this work and the energetic proximity of the minima for a given surface (Figure 6), it is not unreasonable to think that the result obtained in gas phase regarding the interconversion of 2O-Cu_5 structures [33, 34] is similarly achievable here, and therefore we can venture that both 2D and 3D clusters are probably reducible through the 3D isomer along the same lowest energy path. Interestingly, the activation energies for the recombination on NG are very similar

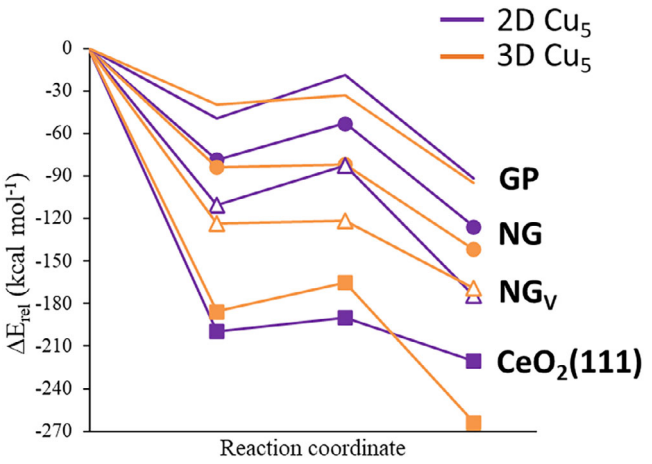

FIGURE 6 | Energy profiles for the O_2 dissociation over 2D (purple) or 3D (orange) Cu_5 clusters in Gas Phase (GP, no markers), and deposited on NG (full dots), NG_V (empty triangles) or $CeO_2(111)$ (full squares). The zero of energy for each surface is: E(2D Cu_5) + E(surface) + E(O_2).

to the ones obtained in gas phase at the PW91 level [33] (73.1 vs 73.1 and 61.8 vs 59.9 kcal mol^{-1} for 2D and 3D Cu_5, respectively, Table 3), whereas for NG_V recombination from 2D and 3D clusters they increase and decrease, respectively, by around 15-20 kcal mol^{-1}. As a result, the NG_V surface favors 3D structures more easily oxidizable, but it is remarkable that even when it does, the 3D isomers are also at least more easily reducible, also in line with the experimental results [34].

On ceria, the tri-coordination of the O atoms on {111} facets in the final state structures is possible and favored (structures **25** and **26**). Indeed, the production of strong O-Cu-O linear interactions with the separate O atoms prevails again, and the clusters are deformed. Reaction energies are again clearly negative, but now the recombination of O_2 from two O atoms, that is, the reduction of the cluster, is not easier in the 3D cluster, but in the planar one (Table 3 and Figure 6). Since the 3D cluster is severely deformed upon dissociation (structure **26**), it is difficult to state whether it would recover the original structure or if the recombination of the molecule may be more easily produced via other geometries for the cluster. Nevertheless, we find again that the isomer that more easily dissociates O_2, planar Cu_5, which is also the more favored thermodynamically, is also the more easily reducible species (Figure 6). Besides, the recombination energy from structure **25** is of 30.4 kcal mol^{-1} only, as opposed to the 73.1 of isolated 2D clusters. Thus, the recombination of 2O atoms back to O_2 may be possible for planar $Cu_5/CeO_2(111)$, but it is unlikely on 3D $Cu_5/CeO_2(111)$.

In summary, N-graphene results confirm that its effect on the copper clusters oxidative performance is low, but even though the MSI is improved with respect to graphene, the material may still suffer from sintering [51], impeding successful industrial application as is. On the other hand, we obtain much higher adsorption energies for the copper clusters on ceria, potentially diminishing the sintering threat. Besides, not only do we find that its strong MSI reverses the behavior of 2D and 3D cluster morphologies, but also that the isomer with the lowest O_2 dissociation barrier, in this case the planar one, is also the more easily reducible. While it is true that there are also other important variables to consider (ceria surface exposed and O vacancies [58], O_2 coverage and dynamics [40, 51, 92]), this reducibility is precisely a key point for the successful catalysis of oxidation reactions, and this conclusion already provides positive evidence for the potential application of Cu_5/CeO_2 catalysts to these reactions.

The practical significance of this for application also depends on how suitable each isomer is for the specific oxidation reaction. In principle, both isomers seem applicable in general: one is more resistant to O_2 dissociation, thus potentially intervening with O_2 in its molecular form, whereas the other easily dissociates O_2 but also easily recombines the molecule, which means it has potential to catalyze oxidation reactions through O* atoms (oxidation is not irreversible). However, the basicity of these O* atoms may still favor competitive reactions, lowering selectivity. This is for instance what we concluded for 3D Cu_5 gas phase clusters regarding propene epoxidation. And this is where the differences between the isomers matter: the 2D cluster showed a viable complete Cu_5-O_2-propene → Cu_5-O*-propene epoxide → Cu_5-2(propene epoxide) catalytic cycle [37].

The opposite structure-activity trend found for ceria is thus relevant because all our previous works pointed to 2D Cu_5 as the more desirable isomer to be stabilized, whereas our 3D Cu_5 ceria results open the door to the applicability of tuned 3D Cu_5 as well. This is still subject to the feasibility of synthesizing clusters of atomicity five and of a specific geometry, but this result further implies that other supported Cu_5 catalysts may be designed to overcome the current limitations for application.

4 | Conclusion

Firstly, we show that the interaction between Cu_5 clusters and clean graphene and N-graphene is weak. Adding nitrogen to graphene enhances the interaction, but proper chemical adsorption is only achieved on the defects explored, namely, C vacancies and three pyridinic N atoms sites. The weak physisorption nevertheless grants Cu_5 clusters a certain stabilization that facilitates their deformation upon the adsorption of a molecule such as O_2. Given this and the energetical proximity of their planar and 3D isomers, interconversion of isomers is commonly observed during calculations, reflecting their fluxionality. In spite of this, the conclusions on N-graphene are very similar to the results obtained in previous works on gas phase clusters, i.e. planar clusters are favored, adsorb O_2 in *bridge* modes and hence are less active towards its dissociation. The three pyridinic N atoms site somewhat favors the 3D isomers thermodynamically, but interconversion from 3D to planar clusters has also been produced at this site.

Regarding $CeO_2(111)$, it is found that the hexagonal symmetry of the surface almost matches the geometry of planar Cu_5, which adds to the strong O-Cu interaction. When clusters are adsorbed on ceria, they get oxidized and produce Ce^{3+} atoms on the surface, whose positions can greatly change the energy of the structure. Nevertheless, the strong interaction and the symmetry matching produces very few geometries close in energy for the Cu_5 clusters, which do not deform into one another in the calculations. Planar clusters adsorb parallel to the surface,

interacting with all five atoms, and the 3D cluster breaks one of its Cu-Cu bonds to interact with four atoms in a rhombus shape, leaving the remaining Cu atom on top of one of the facets. Since planar clusters are not in an upright position anymore, the adsorption of O_2 at its edges is highly impeded. Instead, O_2 is able now to strongly adsorb at the planar Cu_5 *h-111* facets, getting highly activated in the process. In contrast, the molecule prefers a *bridge* site on the opened 3D cluster, and even when a *h-111* mode is close in energy, the copper atoms are not close enough to stabilize both O atoms at the TS, thus yielding a higher activation energy.

Therefore, while on clean N-graphene the properties of the Cu_5 clusters observed from gas phase are kept, supporting them on ceria produces a material with reversed morphology results: 2D Cu_5 clusters are more resistant to oxidation on N-graphene and gas phase, whereas 3D Cu_5 clusters are more resistant on CeO_2(111). Similarly, on N-graphene and gas phase, Cu_5 clusters are more likely to reduce through 3D structures, whereas for ceria the planar structure is the one more easily reducible. The activation of the O_2 molecule still depends on its adsorption mode, but this work shows how the reactivity of copper clusters of a given morphology can be severely changed via the MSI, opening the door to the design of copper catalysts of fine-tuned optimal features.

Acknowledgments

This work was supported by the Spanish Ministry of Science and Innovation (MINECO) through the Severo Ochoa Program (SEV-2016-0683 and CEX2021-001230-S). Red Española de Supercomputación (RES) and Centre de Càlcul de la Universitat de Valencia are gratefully acknowledged for computational resources and technical support. E.F. thanks the Spanish MINECO for her fellowship SVP-2013-068146 and mobility grant EEBB-I-17-12057. The work on Cu_5/CeO_2 was performed during a visit of E. F. at Humboldt Universität. The work at Humboldt Universität was supported by the German Research Foundation (DFG) within the Cluster of Excellence "Unifying Concepts in Catalysis" (EXC314). Part of the calculations were carried out at the facilities of the North-German Supercomputing Alliance HLRN.

Conflicts of Interest

The authors declare no conflicts of interest.

Data Availability Statement

The data that support the findings of this study are available from the corresponding author upon reasonable request.

References

1. M. B. Gawande, A. Goswami, F.-X. Felpin, et al., "Cu and Cu-Based Nanoparticles: Synthesis and Applications in Catalysis," *Chemical Reviews* 116 (2016): 3722, https://doi.org/10.1021/acs.chemrev.5b00482.

2. L. Liu and A. Corma, "Metal Catalysts for Heterogeneous Catalysis: From Single Atoms to Nanoclusters and Nanoparticles," *Chemical Reviews* 118 (2018): 4981, https://doi.org/10.1021/acs.chemrev.7b00776.

3. R. van den Berg, G. Prieto, G. Korpershoek, et al., "Structure Sensitivity of Cu and CuZn Catalysts Relevant to Industrial Methanol Synthesis," *Nature Communications* 7 (2016): 13057, https://doi.org/10.1038/ncomms13057.

4. J. Kim, N. Pfänder, and G. Prieto, "Recycling of CO_2 by Hydrogenation of Carbonate Derivatives to Methanol: Tuning Copper–Oxide Promotion Effects in Supported Catalysts," *ChemSusChem* 13 (2020): 2043, https://doi.org/10.1002/cssc.202000166.

5. R. Singh, V. Pandey, and K. K. Pant, "Promotional Role of Oxygen Vacancy Defects and Cu−Ce Interfacial Sites on the Activity of Cu/CeO_2 Catalyst for CO_2 Hydrogenation to Methanol," *ChemCatChem* 14 (2022): e202201053, https://doi.org/10.1002/cctc.202201053.

6. E. Fernández-Villanueva, P. G. Lustemberg, M. Zhao, J. Soriano Rodriguez, P. Concepción, and M. V. Ganduglia-Pirovano, "Water and Cu+ Synergy in Selective CO_2 Hydrogenation to Methanol over Cu-MgO-Al_2O_3 Catalysts," *Journal of the American Chemical Society* 146 (2024): 2024, https://doi.org/10.1021/jacs.3c10685.

7. I. López-Luque, J. Hack, T. Ródenas, et al., "Engineering Peripheral Metal-Oxide Catalysis: Interparticle Spacing in Cu/ZrO_2 Catalysts for Methanol Synthesis by CO_2 Hydrogenation," *Angewandte Chemie International Edition* 64 (2025): e202420126, https://doi.org/10.1002/anie.202420126.

8. P. Ren, Z. Zhang, T. Hu, et al., "Reactants-Driven Surface-Active Sites on a Cu/CeO_2 Catalyst for Methanol Synthesis from Syngas," *ChemCatChem* 17 (2025): e202401425, https://doi.org/10.1002/cctc.202401425.

9. D. A. A. Jurado, M. D. Higham, Y. R. Poh, C. R. A. Catlow, and I. Krossing, "Mechanism of CO2 Conversion to Methanol on a Highly Representative Model Cu/ZnO Interface," *Journal of Catalysis* 446 (2025): 115997, https://doi.org/10.1016/j.jcat.2025.115997.

10. M. Monte, D. Gamarra, A. L. Cámara, et al., "Preferential Oxidation of CO in Excess H_2 over CuO/CeO_2 Catalysts: Performance as a Function of the Copper Coverage and Exposed Face Present in the CeO_2 Support," *Catalysis Today* 229 (2014): 104, https://doi.org/10.1016/j.cattod.2013.10.078.

11. W.-W. Wang, W.-Z. Yu, P.-P. Du, et al., "Crystal Plane Effect of Ceria on Supported Copper Oxide Cluster Catalyst for CO Oxidation: Importance of Metal–Support Interaction," *ACS Catalysis* 7 (2017): 1313, https://doi.org/10.1021/acscatal.6b03234.

12. W. Ji, X. Chen, Q. Li, K. Lin, J. Deng, and X. Xing, "Insights into CO Oxidation in Cu/CeO_2 Catalysts: O_2 Activation at the Dual-Interfacial Sites," *European Journal of Inorganic Chemistry* 26 (2023): e202200656, https://doi.org/10.1002/ejic.202200656.

13. L. Zhang, J. Pan, M. Li, I. A. W. Filot, E. J. M. Hensen, and H. Wang, "Effect of Reaction Atmosphere on Catalytic CO Oxidation over Cu-Based Bimetallic Nanoclusters on a CeO_2 Support," *Physical Review Applied* 20 (2023): 34051, https://doi.org/10.1103/PhysRevApplied.20.034051.

14. X. Hou, Q. Zhao, X. Liu, et al., "CeO_2 Crystal Plane Engineering to Modulate CuO-CeO_2 Interactions and Modify the CO-PROX Reaction Pathway," *Chemical Engineering Journal* 480 (2024): 147982, https://doi.org/10.1016/j.cej.2023.147982.

15. D. Liu, H. Zhu, X. Gong, et al., "Boosting CO Oxidation Performance via Reaction-induced Single-atom Active Site: DFT and Microkinetic Investigation of a Unified CO Oxidation Mechanism on Gd-doped Ceria-supported Copper Catalysts," *Journal of Rare Earths* 43 (2025): 1870, https://doi.org/10.1016/j.jre.2024.09.015.

16. L. Du, W. Wang, H. Yan, et al., "Copper-ceria Sheets Catalysts: Effect of Copper Species on Catalytic Activity in CO Oxidation Reaction," *Journal of Rare Earths* 35 (2017): 1186, https://doi.org/10.1016/j.jre.2017.04.005.

17. Z. Yang, L. Xie, D. Ma, and G. Wang, "Origin of the High Activity of the Ceria-Supported Copper Catalyst for H_2O Dissociation," *The Journal of Physical Chemistry C* 115 (2011): 6730, https://doi.org/10.1021/jp200005r.

18. Y.-C. Chen and G.-C. Wang, "Structure Sensitivity of the Water–Gas Shift Reaction over Cu/CeO_2: A Combination of DFT, MF-MKM, and kMC," *The Journal of Physical Chemistry C* 128 (2024): 9926, https://doi.org/10.1021/acs.jpcc.4c01539.

19. Y.-X. Zhu, Y. Wang, and G.-C. Wang, "Key Role of Yttrium Doping on Cu/CeO2 (111) in Water–gas Shift Reaction: Promotion of Cluster

Dispersity," *Journal of Catalysis* 451 (2025): 116405, https://doi.org/10.1016/j.jcat.2025.116405.

20. F. Meng, M. Peng, Y. Chen, et al., "Defect-rich Graphene Stabilized Atomically Dispersed Cu_3 Clusters with Enhanced Oxidase-Like Activity for Antibacterial Applications," *Applied Catalysis B: Environmental* 301 (2022): 120826, https://doi.org/10.1016/j.apcatb.2021.120826.

21. X.-J. Cui, Y.-Q. Qiu, H.-Q. Wang, and C.-G. Liu, "Direct Coupling of Two Inert CO_2 Molecules to Form a C–C Bond on the Cu0 Atomic Interfaces of the Nitrogen-doped Graphene-supported Cu_4 Cluster," *Inorganic Chemistry Frontiers* 11 (2024): 85, https://doi.org/10.1039/D3QI02000B.

22. T. Xiao, Z. Yang, H. Wu, et al., "Size Dependence over Cu-based Catalysts for Semi-hydrogenation of Symmetric-structured Molecules," *Journal of Catalysis* 449 (2025): 116225, https://doi.org/10.1016/j.jcat.2025.116225.

23. Y. Song, R. Peng, D. K. Hensley, et al., "High-Selectivity Electrochemical Conversion of CO_2 to Ethanol Using a Copper Nanoparticle/N-Doped Graphene Electrode," *ChemistrySelect* 1 (2016): 6055.

24. M. Zhang, X. Xuan, W. Wang, C. Ma, and Z. Lin, "Anode Photovoltage Compensation-Enabled Synergistic CO_2 Photoelectrocatalytic Reduction on a Flower-like Graphene-Decorated Cu Foam Cathode," *Advanced Functional Materials* 30 (2020): 2005983, https://doi.org/10.1002/adfm.202005983.

25. R. Saini, F. Naaz, A. H. Bashal, A. H. Pandit, and U. Farooq, "Recent Advances in Nitrogen-doped Graphene-based Heterostructures and Composites: Mechanism and Active Sites for Electrochemical ORR and HER," *Green Chemistry* 26 (2024): 57.

26. E. Fernández and M. Boronat, "Sub Nanometer Clusters in Catalysis," *Journal of Physics: Condensed Matter* 31 (2019): 13002.

27. C. Dong, Y. Li, D. Cheng, et al., "Supported Metal Clusters: Fabrication and Application in Heterogeneous Catalysis," *ACS Catalysis* 10 (2020): 11011, https://doi.org/10.1021/acscatal.0c02818.

28. H. Rong, S. Ji, J. Zhang, D. Wang, and Y. Li, "Synthetic Strategies of Supported Atomic Clusters for Heterogeneous Catalysis," *Nature Communications* 11 (2020): 5884, https://doi.org/10.1038/s41467-020-19571-6.

29. M. P. de Lara-Castells, "An Ab Initio Journey toward the Molecular-Level Understanding and Predictability of Subnanometric Metal Clusters," *Small Structures* 5 (2024): 2400147, https://doi.org/10.1002/sstr.202400147.

30. Z. Luo and A. Shehzad, "Advances in Naked Metal Clusters for Catalysis," *ChemPhysChem* 25 (2024): e202300715, https://doi.org/10.1002/cphc.202300715.

31. M. Chen, C. Guo, L. Qin, et al., "Atomically Precise Cu Nanoclusters: Recent Advances, Challenges, and Perspectives in Synthesis and Catalytic Applications," *Nanomicro Lett* 17 (2024): 83.

32. S. Wang, C. Liu, W. Hao, et al., "Structural Evolution of Metal Single-atoms and Clusters in Catalysis: Which Are the Active Sites under Operative Conditions?," *Chemical Science* 16 (2025): 6203, https://doi.org/10.1039/D5SC01221J.

33. E. Fernández, M. Boronat, and A. Corma, "Trends in the Reactivity of Molecular O_2 with Copper Clusters: Influence of Size and Shape," *The Journal of Physical Chemistry C* 119 (2015): 19832, https://doi.org/10.1021/acs.jpcc.5b05023.

34. P. Concepcion, M. Boronat, S. Garcia-Garcia, E. Fernandez, and A. Corma, "Enhanced Stability of Cu Clusters of Low Atomicity against Oxidation. Effect on the Catalytic Redox Process," *ACS Catalysis* 7 (2017): 3560, https://doi.org/10.1021/acscatal.7b00778.

35. D. Buceta, S. Huseyinova, M. Cuerva, et al., "Stability and Reversible Oxidation of Sub-Nanometric Cu5 Metal Clusters: Integrated Experimental Study and Theoretical Modeling," *Chemistry—A European Journal* 29 (2023): e202301517.

36. E. Fernández, M. Boronat, and A. Corma, "The 2D or 3D Morphology of Sub-nanometer Cu_5 and Cu_8 Clusters Changes the Mechanism of CO Oxidation," *Physical Chemistry Chemical Physics* 24 (2022): 4504, https://doi.org/10.1039/D1CP05166K.

37. E. Fernández, M. Boronat, and A. Corma, "The Crucial Role of Cluster Morphology on the Epoxidation of Propene Catalyzed by Cu_5: A DFT Study," *The Journal of Physical Chemistry C* 124 (2020): 21549, https://doi.org/10.1021/acs.jpcc.0c06295.

38. M. Gallego, A. Corma, and M. Boronat, "Sub-nanometer Copper Clusters as Alternative Catalysts for the Selective Oxidation of Methane to Methanol with Molecular O_2," *The Journal of Physical Chemistry A* 126 (2022): 4941, https://doi.org/10.1021/acs.jpca.2c02895.

39. Q. Wan, F. Wei, Y. Wang, et al., "Single Atom Detachment from Cu Clusters, and Diffusion and Trapping on CeO_2(111): Implications in Ostwald Ripening and Atomic Redispersion," *Nanoscale* 10 (2018): 17893, https://doi.org/10.1039/C8NR06232C.

40. H. Guo, P. Poths, P. Sautet, and A. N. Alexandrova, "Oxidation Dynamics of Supported Catalytic Cu Clusters: Coupling to Fluxionality," *ACS Catalysis* 12 (2022): 818, https://doi.org/10.1021/acscatal.1c04100.

41. M. Gallego, A. Corma, and M. Boronat, "Influence of the Zeolite Support on the Catalytic Properties of Confined Metal Clusters: A Periodic DFT Study of O_2 Dissociation on Cun Clusters in CHA," *Physical Chemistry Chemical Physics* 24 (2022): 30044, https://doi.org/10.1039/D2CP04915E.

42. M. Gallego, A. Corma, and M. Boronat, "An Alternative Catalytic Cycle for Selective Methane Oxidation to Methanol with Cu Clusters in Zeolites," *Physical Chemistry Chemical Physics* 26 (2024): 5914, https://doi.org/10.1039/D3CP05802F.

43. K. M. Krupka, L. L. Carroll, and M. P. de Lara-Castells, "Functionalization of Zeolite-encapsulated Cu_5 Clusters as Visible-light Photoactive Sub-nanomaterials," *RSC Advances* 15 (2025): 2086, https://doi.org/10.1039/D4RA08633C.

44. E. F. Villanueva, "Theoretical Study of the Geometrical, Electronic and Catalytic Properties of Metal Clusters and Nanoparticles" [PhD thesis] Universitat Politècnica de València 2019, https://doi.org/10.4995/Thesis/10251/135277.

45. P. Jain, R. S. Rajput, S. Kumar, et al., "Recent Advances in Graphene-Enabled Materials for Photovoltaic Applications: A Comprehensive Review," *ACS Omega* 9 (2024): 12403.

46. X. Xue, S. Li, and M. Zhu, "Recent Progress in Graphene-based Materials for Thermoelectric Applications," *RSC Advance* 15 (2025): 26919.

47. H. Wang, T. Maiyalagan, and X. Wang, "Review on Recent Progress in Nitrogen-Doped Graphene: Synthesis, Characterization, and Its Potential Applications," *ACS Catalysis* 2 (2012): 781, https://doi.org/10.1021/cs200652y.

48. P. Błoński, J. Tuček, Z. Sofer, et al., "Doping with Graphitic Nitrogen Triggers Ferromagnetism in Graphene," *Journal of the American Chemical Society* 139 (2017): 3171.

49. D. A. Bulushev, A. L. Chuvilin, V. I. Sobolev, et al., "Copper on Carbon Materials: Stabilization by Nitrogen Doping," *Journal of Materials Chemistry A* 5 (2017): 10574, https://doi.org/10.1039/C7TA02282D.

50. D. E. García-Rodríguez, L. H. Mendoza-Huizar, and C. Díaz, "A DFT Study of Cu Nanoparticles Adsorbed on Defective Graphene," *Applied Surface Science* 412 (2017): 146, https://doi.org/10.1016/j.apsusc.2017.03.239.

51. L. L. Carroll, L. V. Moskaleva, and M. P. de Lara-Castells, "Carbon Vacancy-assisted Stabilization of Individual Cu_5 Clusters on Graphene. Insights from Ab Initio Molecular Dynamics," *Physical Chemistry Chemical Physics* 25 (2023): 15729, https://doi.org/10.1039/D2CP05843J.

52. J. Paier, C. Penschke, and J. Sauer, "Oxygen Defects and Surface Chemistry of Ceria: Quantum Chemical Studies Compared to Experiment," *Chemical Reviews* 113 (2013): 3949, https://doi.org/10.1021/cr3004949.

53. T. Montini, M. Melchionna, M. Monai, and P. Fornasiero, "Fundamentals and Catalytic Applications of CeO_2-Based Materials," *Chemical Reviews* 116 (2016): 5987, https://doi.org/10.1021/acs.chemrev.5b00603.

54. P. Li, X. Chen, Y. Li, and J. W. Schwank, "A Review on Oxygen Storage Capacity of CeO_2-based Materials: Influence Factors, Measurement Techniques, and Applications in Reactions Related to Catalytic Automotive Emissions Control," *Catalysis Today* 327 (2019): 90, https://doi.org/10.1016/j.cattod.2018.05.059.

55. S. Laursen, D. Combita, A. B. Hungría, M. Boronat, and A. Corma, "First-Principles Design of Highly Active and Selective Catalysts for Phosgene-Free Synthesis of Aromatic Polyurethanes," *Angewandte Chemie International Edition* 51 (2012): 4190, https://doi.org/10.1002/anie.201108849.

56. S. Agarwal, L. Lefferts, B. L. Mojet, et al., "Exposed Surfaces on Shape-Controlled Ceria Nanoparticles Revealed through AC-TEM and Water–Gas Shift Reactivity," *ChemSusChem* 6 (2013): 1898, https://doi.org/10.1002/cssc.201300651.

57. T. López-Ausens, M. Boronat, P. Concepción, S. Chouzier, S. Mastroianni, and A. Corma, "A Heterogeneous Mechanism for the Catalytic Decomposition of Hydroperoxides and Oxidation of Alkanes over CeO_2 Nanoparticles: A Combined Theoretical and Experimental Study," *Journal of Catalysis* 344 (2016): 334, https://doi.org/10.1016/j.jcat.2016.09.032.

58. C. Yang, X. Yu, S. Heißler, et al., "O_2 Activation on Ceria Catalysts—The Importance of Substrate Crystallographic Orientation," *Angewandte Chemie International Edition* 56 (2017): 16399, https://doi.org/10.1002/anie.201709199.

59. M. J. Manto, P. Xie, and C. Wang, "Catalytic Dephosphorylation Using Ceria Nanocrystals," *ACS Catalysis* 7 (2017): 1931, https://doi.org/10.1021/acscatal.6b03472.

60. P. G. Lustemberg, C. Yang, Y. Wang, M. V. Ganduglia-Pirovano, and C. Wöll, "Synergistic Effects in Low-Temperature CO Oxidation on Cerium Oxide Surfaces," *Journal of the American Chemical Society* 147 (2025): 6958, https://doi.org/10.1021/jacs.4c17658.

61. M. Melchionna and P. Fornasiero, "The Role of Ceria/Precious Metal Interfaces in Catalysis," *RSC Applied Interfaces* 1 (2024): 70, https://doi.org/10.1039/D3LF00202K.

62. M. Wang, Y. Xie, M. Fang, et al., "Promoted Electrochemical CO_2 Methanation over Ultrastable Cu(II)-VO Pair Sites in Cu-CeO_2 Catalyst: Water Activation and Intermediate Adsorption Tuning," *Journal of the American Chemical Society* 147 (2025): 44781, https://doi.org/10.1021/jacs.5c09230.

63. F. Huang, A. Xu, X. Chen, et al., "Constructing f-p-d Orbital Coupling Using Cu-Doped Frustrated Lewis Acid–Base Pairs in CeO2 to Boost CO2 Electroreduction," *ACS Catalysis* 15 (2025): 20864, https://doi.org/10.1021/acscatal.5c05762.

64. E. Fernández-Villanueva, P. Pérez-Bailac, P. G. Lustemberg, et al., "Fine-Tuning Catalysts: The Role of Support Nanomorphology in Shaping Cu/CeO_2 CO-PROX Properties," *ACS Catalysis* 15 (2025): 20360, https://doi.org/10.1021/acscatal.5c06552.

65. W. Wang, Z. Qu, L. Song, and Q. Fu, "CO_2 Hydrogenation to Methanol over Cu/CeO_2 and Cu/ZrO_2 Catalysts: Tuning Methanol Selectivity via Metal-support Interaction," *Journal of Energy Chemistry* 40 (2020): 22, https://doi.org/10.1016/j.jechem.2019.03.001.

66. Y. Zeng, K.-G. Haw, Z. Wang, et al., "Double Redox Process to Synthesize CuO–CeO_2 Catalysts with Strong Cu–Ce Interaction for Efficient Toluene Oxidation," *Journal of Hazardous Materials* 404 (2021): 124088, https://doi.org/10.1016/j.jhazmat.2020.124088.

67. L. Du, L. He, S. Hu, et al., "Tailoring Cu–CeO_2 Catalysts to Elucidate the Morphology–activity Relationship in Low-temperature Water–gas Shift Reaction," *Journal of Colloid and Interface Science* 704 (2026): 139458, https://doi.org/10.1016/j.jcis.2025.139458.

68. B. Zhang, S. Huang, Y. Li, J. Shen, X. Tian, and M. Ding, "Highly Dispersed Cu on Hollow Spherical CeO_2: An Efficient and Stable Catalyst for the RWGS Reaction," *Applied Catalysis B: Environment and Energy* 366 (2025): 125003, https://doi.org/10.1016/j.apcatb.2024.125003.

69. J. P. Perdew, K. Burke, and M. Ernzerhof, "Generalized Gradient Approximation Made Simple," *Physical Review Letters* 77 (1996): 3865, https://doi.org/10.1103/PhysRevLett.77.3865.

70. G. Kresse and J. Furthmuller, "Efficient Iterative Schemes for Ab Initio Total-energy Calculations Using a Plane-wave Basis Set," *Physical Review B* 54 (1996): 11169, https://doi.org/10.1103/PhysRevB.54.11169.

71. G. Kresse and D. Joubert, "From Ultrasoft Pseudopotentials to the Projector Augmented-wave Method," *Physical Review B* 59 (1999): 1758, https://doi.org/10.1103/PhysRevB.59.1758.

72. S. L. Dudarev, G. A. Botton, S. Y. Savrasov, C. J. Humphreys, and A. P. Sutton, "Electron-energy-loss Spectra and the Structural Stability of Nickel Oxide:an LSDA+U Study," *Physical Review B* 57 (1998): 1505, https://doi.org/10.1103/PhysRevB.57.1505.

73. S. Fabris, G. Vicario, G. Balducci, S. D. Gironcoli, and S. Baroni, "Electronic and Atomistic Structures of Clean and Reduced Ceria Surfaces," *The Journal of Physical Chemistry B* 109 (2005): 22860, https://doi.org/10.1021/jp0511698.

74. M. Cococcioni and S. D. Gironcoli, "Linear Response Approach to the Calculation of the Effective Interaction Parameters in the LDA+U Method," *Physical Review B* 71 (2005): 35105, https://doi.org/10.1103/PhysRevB.71.035105.

75. C. W. M. Castleton, J. Kullgren, and K. Hermansson, "Tuning LDA+U for Electron Localization and Structure at Oxygen Vacancies in Ceria," *The Journal of Chemical Physics* 127 (2007): 244704, https://doi.org/10.1063/1.2800015.

76. P. E. Blöchl, "Projector Augmented-Wave Method," *Physical Review B* 50 (1994): 17953.

77. A. Pulido, M. Boronat, and A. Corma, "Theoretical Investigation of Gold Clusters Supported on Graphene Sheets," *New Journal of Chemistry* 35 (2011): 2153, https://doi.org/10.1039/c1nj20215d.

78. H. J. Monkhorst and J. D. Pack, "Special Points for Brillouin-zone Integrations," *Physical Review B* 13 (1976): 5188, https://doi.org/10.1103/PhysRevB.13.5188.

79. W. Tang, E. Sanville, and G. Henkelman, "A Grid-based Bader Analysis Algorithm without Lattice Bias," *Journal of Physics: Condensed Matter* 21 (2009): 84204.

80. E. Sanville, S. D. Kenny, R. Smith, and G. Henkelman, "Improved Grid-Based Algorithm for Bader Charge Allocation," *Journal of Computational Chemistry* 28 (2007): 899, https://doi.org/10.1002/jcc.20575.

81. G. Henkelman, A. Arnaldsson, and H. Jónsson, "A Fast and Robust Algorithm for Bader Decomposition of Charge Density," *Computational Materials Science* 36 (2006): 354, https://doi.org/10.1016/j.commatsci.2005.04.010.

82. S. Grimme, "Semiempirical GGA-Type Density Functional Constructed with a Long-Range Dispersion Correction," *Journal of Computational Chemistry* 27 (2006): 1787, https://doi.org/10.1002/jcc.20495.

83. C. Penschke, J. Paier, and J. Sauer, "Oligomeric Vanadium Oxide Species Supported on the CeO_2(111) Surface: Structure and Reactivity Studied by Density Functional Theory," *The Journal of Physical Chemistry C* 117 (2013): 5274, https://doi.org/10.1021/jp400520j.

84. G. Henkelman and H. Jónsson, "A Dimer Method for Finding Saddle Points on High Dimensional Potential Surfaces Using Only First Derivatives," *The Journal of Chemical Physics* 111 (1999): 7010, https://doi.org/10.1063/1.480097.

85. A. Heyden, A. T. Bell, and F. J. Keil, "Efficient Methods for Finding Transition States in Chemical Reactions: Comparison of Improved Dimer Method and Partitioned Rational Function Optimization Method," *The Journal of Chemical Physics* 123 (2005): 224101, https://doi.org/10.1063/1.2104507.

86. G. Henkelman, B. P. Uberuaga, and H. Jónsson, "A Climbing Image Nudged Elastic Band Method for Finding Saddle Points and Minimum Energy Paths," *The Journal of Chemical Physics* 113 (2000): 9901, https://doi.org/10.1063/1.1329672.

87. "Jmol: un Visor Java de Código Abierto para Estructuras Químicas en Tres Dimensiones," http://www.jmol.org/.

88. "p4vasp", http://www.p4vasp.at/.

89. K. Momma and F. Izumi, "VESTA 3 for Three-dimensional Visualization of Crystal, Volumetric and Morphology Data," *Journal of Applied Crystallography* 44 (2011): 1272, https://doi.org/10.1107/S0021889811038970.

90. https://sourceforge.net/projects/qtgrace/.

91. G. Feng, M. V. Ganduglia-Pirovano, C.-F. Huo, and J. Sauer, "Hydrogen Spillover to Copper Clusters on Hydroxylated γ-Al_2O_3," *The Journal of Physical Chemistry C* 122 (2018): 18445, https://doi.org/10.1021/acs.jpcc.8b03764.

92. Q. Wu, S. Hou, D. Buceta, H. J. L. Ordoñez, M. A. López-Quintela, and C. J. Lambert, "Tuning the Surface States of TiO_2 Using Cu_5 Atomic Clusters," *Applied Surface Science* 594 (2022): 153455, https://doi.org/10.1016/j.apsusc.2022.153455.

93. Y. Chen, X. Yang, Y. Liu, J. Zhao, Q. Cai, and X. Wang, "Can Si-doped Graphene Activate or Dissociate O_2 Molecule?," *Journal of Molecular Graphics and Modelling* 39 (2013): 126, https://doi.org/10.1016/j.jmgm.2012.11.009.

94. S. Ni, Z. Li, and J. Yang, "Oxygen Molecule Dissociation on Carbon Nanostructures with Different Types of Nitrogen Doping," *Nanoscale* 4 (2012): 1184, https://doi.org/10.1039/C1NR11086A.

95. A. H. C. Neto, F. Guinea, N. M. R. Peres, K. S. Novoselov, and A. K. Geim, "The Electronic Properties of Graphene," *Reviews of Modern Physics* 81 (2009): 109–162, https://doi.org/10.1103/RevModPhys.81.109.

Supporting Information

Additional supporting information can be found online in the Supporting Information section.

The authors have cited additional references within the Supporting Information [95].

Supporting File: cctc70547-sup-0001-SuppMat.docx.